

CANDU Lattice Uncertainties During Burnup

M. R. Ball¹, D. R. Novog² and J.C. Luxat³

McMaster University, Ontario, Canada

¹ballmr@mcmaster.ca

²novog@mcmaster.ca

³luxatj@mcmaster.ca

Abstract

Uncertainties associated with fundamental nuclear data accompany evaluated nuclear data libraries in the form of covariance matrices. As nuclear data are important parameters in reactor physics calculations, any associated uncertainty causes a loss of confidence in the calculation results. The quantification of output uncertainties is necessary to adequately establish safety margins of nuclear facilities. In this work, microscopic cross-section has been propagated through lattice burnup calculations applied to a generic CANDU[®] model. It was found that substantial uncertainty emerges during burnup even when fission yield fraction and decay rate uncertainties are neglected.

1. Introduction

Lattice physics calculations depend on many parameters whose values cannot be precisely known. Examples include fundamental nuclear data (e.g. neutron cross-sections) and operational parameters such as coolant temperature and density. The uncertainty associated with the lattice parameters causes a loss of confidence in the lattice calculation results. While lattice physics uncertainty analysis is being studied with increasing interest by academia, industry, and regulatory authorities[1], the investigations tend to be focused on temporal snapshots of the system. Literature on the subject of lattice uncertainty typically involves an analysis of systems with static, best-estimate fuel compositions, which corresponds to Beginning of Cycle (BoC), End of Cycle (EoC), or some particular point of mid-burnup. From that static, instantaneous fuel composition, analyses can be conducted to evaluate the uncertainty in lattice responses that result from the nuclear data of the isotopes which are present in the fuel in various quantities at that instant.

However, uncertainty analysis applied to such static models neglects the uncertainty effects that emerge only in a temporal context, namely, that the best-estimate fuel composition at any point during burnup is also uncertain. Immediately from the onset of burnup, uncertainty exists in reaction rates for all nuclides. A nuclide's reaction rate uncertainty results directly from its own cross-section uncertainty as well as indirectly from the uncertainty in the neutron flux, which itself depends on reaction rate uncertainties of all system nuclides. Consequently, as the production rates of fission and activation products are uncertain, so is the accumulated bundle inventory of those product nuclides as the bundle is further burned. In a discrete-time setting (which is appropriate to numerical lattice physics calculation), the evolution of lattice uncertainties can be described by the flowchart shown in Figure 1.

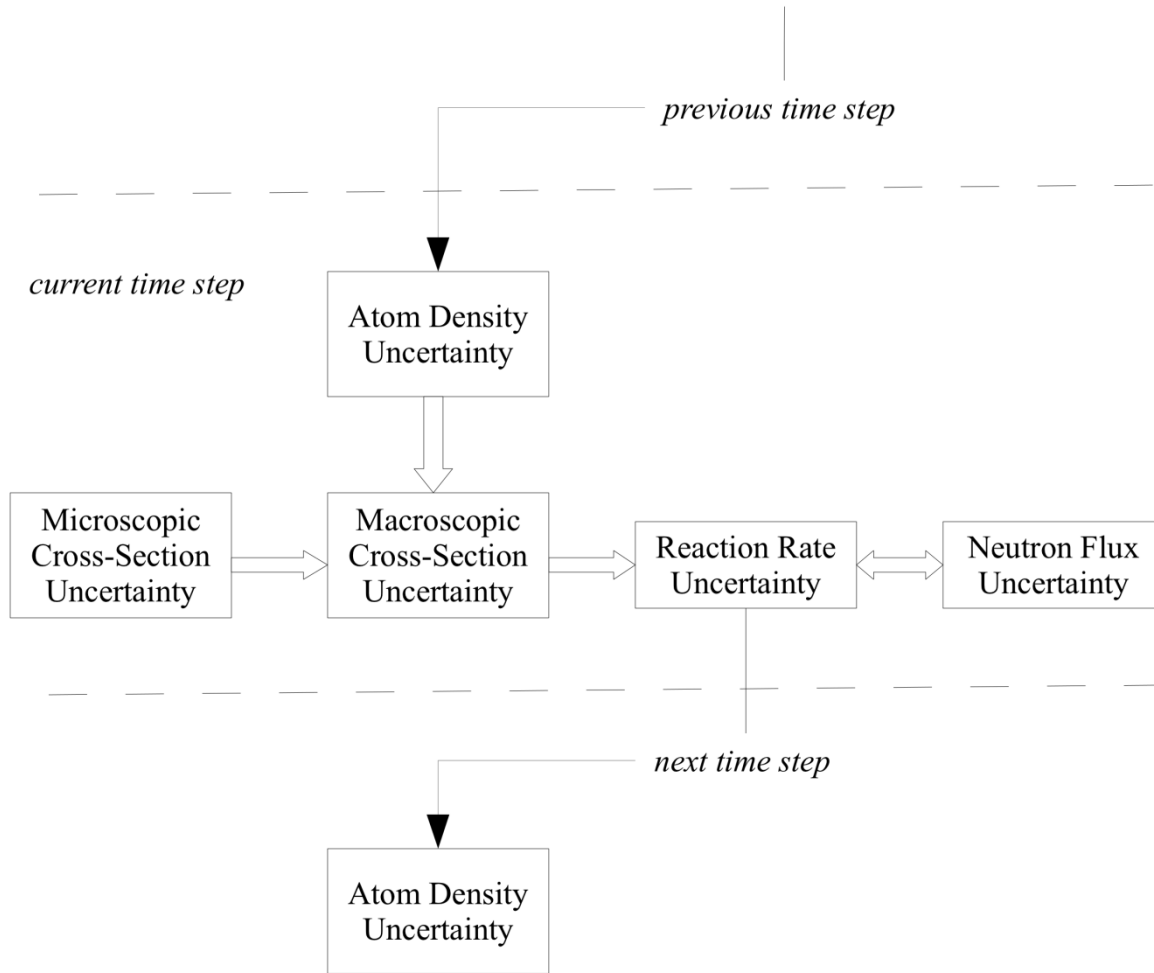


Figure 1 Burnup Uncertainty Flowchart

Lattice uncertainties compound with additional burnup, and therefore the confidence associated with atom density and neutron flux predictions tends to decrease. It will be shown in subsequent sections that, after exhibiting a local minimum, the relative uncertainty of a CANDU[®] lattice k_{∞} increases monotonically with increasing bundle irradiation.

2. Uncertainty Propagation Methodology

A statistical sampling uncertainty propagation technique was developed for performing the uncertainty analysis described in this paper. A detailed description of its development is available elsewhere[2], but is summarized in this section.

2.1 Uncertainty Source Data

Lattice physics uncertainty analysis depends on quantified uncertainty information associated with the fundamental nuclear data of the nuclides relevant to the lattice. As of ENDF/B-VI[3], such uncertainty data is included in the ENDF library format in the form of covariance matrices. Covariance is a statistical measure of the distribution of dependent random variables – in this case, nuclear cross-sections. Each energy group value of each cross-section of each nuclide is considered a dependent random variable for the purposes of defining their corresponding covariance matrix. The definition of covariance between two variables is shown in equation (1). When considering the covariance of a variable with itself, note that equation (1) reduces merely to the variance of the variable.

$$cov(x, y) \equiv E[(x - E(x))(y - E(y))] \quad (1)$$

The base covariance matrix used in this work was evaluated by Oak Ridge National Laboratory (ORNL) based primarily on ENDF/B-VI data, and compiled to a covariance library called 44GROUPV6REC[4]. The covariance library is in a 44-group energy structure, and includes covariance data for over 300 nuclides and a variety of ENDF Section (MT) cross-sections/parameters shown in Table 1.

MT	Parameter
1	(n, total)
2	(n, n ₀)
4	(n, n'γ)
16	(n, 2n)
18	(n, f)
102	(n, γ)
103	(n, p)
104	(n, d)
105	(n, t)
106	(n, He ³)
107	(n, α)
452	$\bar{\nu}$
1018	χ

Table 1 MTs supported by 44GROUPV6REC

As each parameter in Table 1 is discretized in 44 energy groups, there are therefore 44 dependent random variables per parameter – which correspond to each group value. Each dependent variable, following some statistical distribution, has an associated variance. To the extent that some energy group values of a parameter have some manner of mutual dependency (for example, cross-sections that follow a $1/v$ relationship at thermal energies), covariance exists between the energy values of a

parameter. Moreover, covariance often exists between parameters belonging to the same nuclide, and even between parameters belonging to different nuclides.

2.1.1 Covariance Interpolation

When quantifying the uncertainty associated with best-estimate predictions, the covariance matrix should be of an identical energy group structure as the reference nuclear data used to generate the best-estimate solutions. In the case of this work, the lattice code used was DRAGON 3.06J [5], using 69-group WIMS-D4 format nuclear data library produced by the International Atomic Energy Agency (IAEA) through its WIMS Library Update Project (WLUP) [6]. The IAEA data library is available from the WLUP website.

The 44GROUPV6REC covariance library, therefore, was interpolated to the 69-group WLUP energy structure using the code ANGELO2 [7]. The resulting covariance library, deemed here as 69GROUPV6REC, contains interpolated data that is approximately equivalent to that of 44GROUPV6REC, but lacking any covariance information between different nuclides. The loss of nuclide-to-nuclide uncertainty is due to limitations of ANGELO2.

2.2 **Uncertainty Propagation by Statistical Sampling**

Recall that each uncertain parameter is considered to be a dependent, random variable. Random implies that the variables can take on different values according to a probability distribution function, while their dependency requires that values of some variables cannot be considered without regard to those of other variables. The underlying method to the uncertainty propagation technique used in this work is to perform a Monte Carlo sampling of each dependent random variable (uncertain parameter) according to its statistical distribution, and therefore randomly generate sets of new data. For each randomly sampled set of parameters, there exists a corresponding set of outputs which are the solution to the lattice physics equations acting on the input sample. When many samples are taken, a distribution of output responses emerges that characterizes the uncertainty of those outputs that arises from the uncertainty of the inputs being sampled.

To perform a statistical sampling of an input parameter, several of the parameter's statistical moments must be known: the mean of the parameter, the variance/covariance of the parameter, and the shape of the distribution. In this work, the mean of each parameter is taken to be the reference multi-group value that is found in the 69-group WLUP data library. The variance/covariance is found in 69GROUPV6REC which is an interpolated value from the ORNL evaluation. The higher statistical moments that characterize the shape of the distribution (i.e. Gaussian, uniform, etc.) must be assumed, and in this work the distributions are assumed to be uniform. A thorough comparison between the assumptions of Gaussian distributions and uniform distributions in the context of lattice uncertainty analysis has been previously detailed by the author elsewhere[2].

As an example, observe Figure 2 showing the reference best-estimate 69-group cross-section of Pu²³⁹ (n, γ) in contrast to 256 statistical samples of the same. The sampling was done so that the

collective statistics of the samples are entirely consistent with the cross-section's 69-group covariance matrix shown in Figure 3.

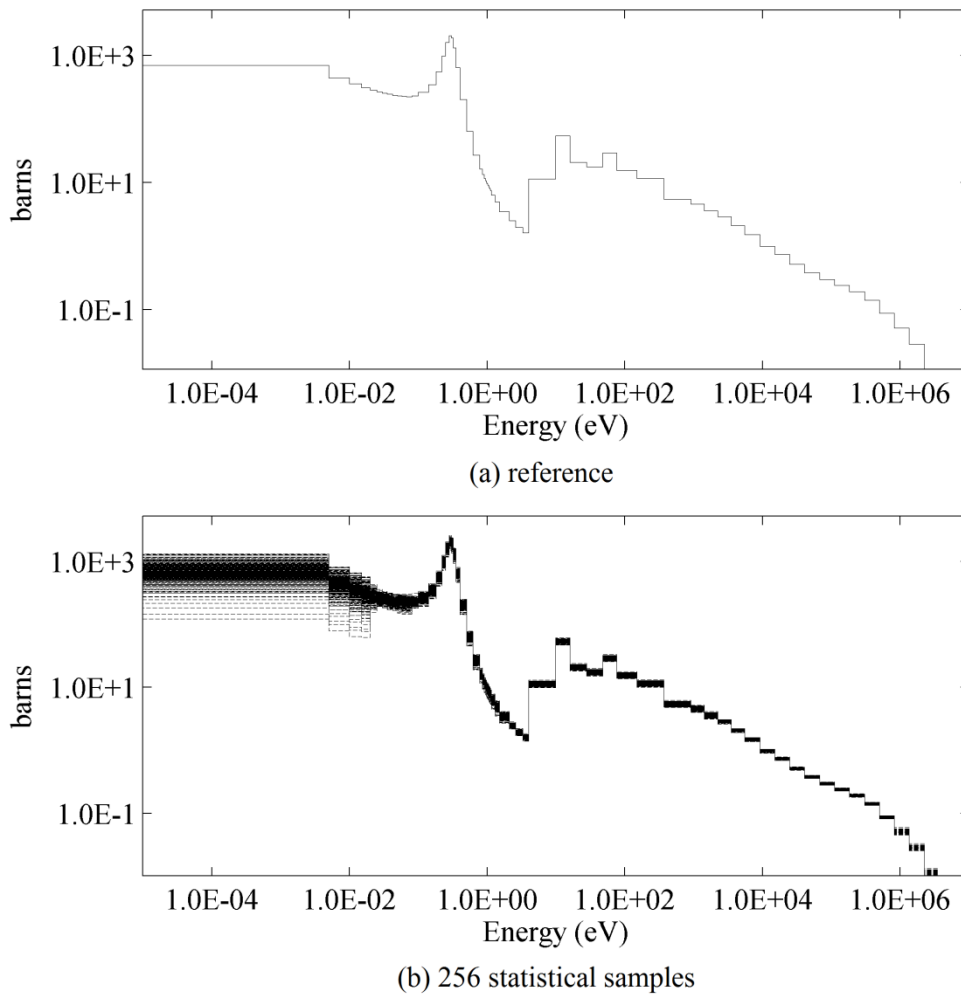


Figure 2 Pu^{239} (n, γ) cross-section

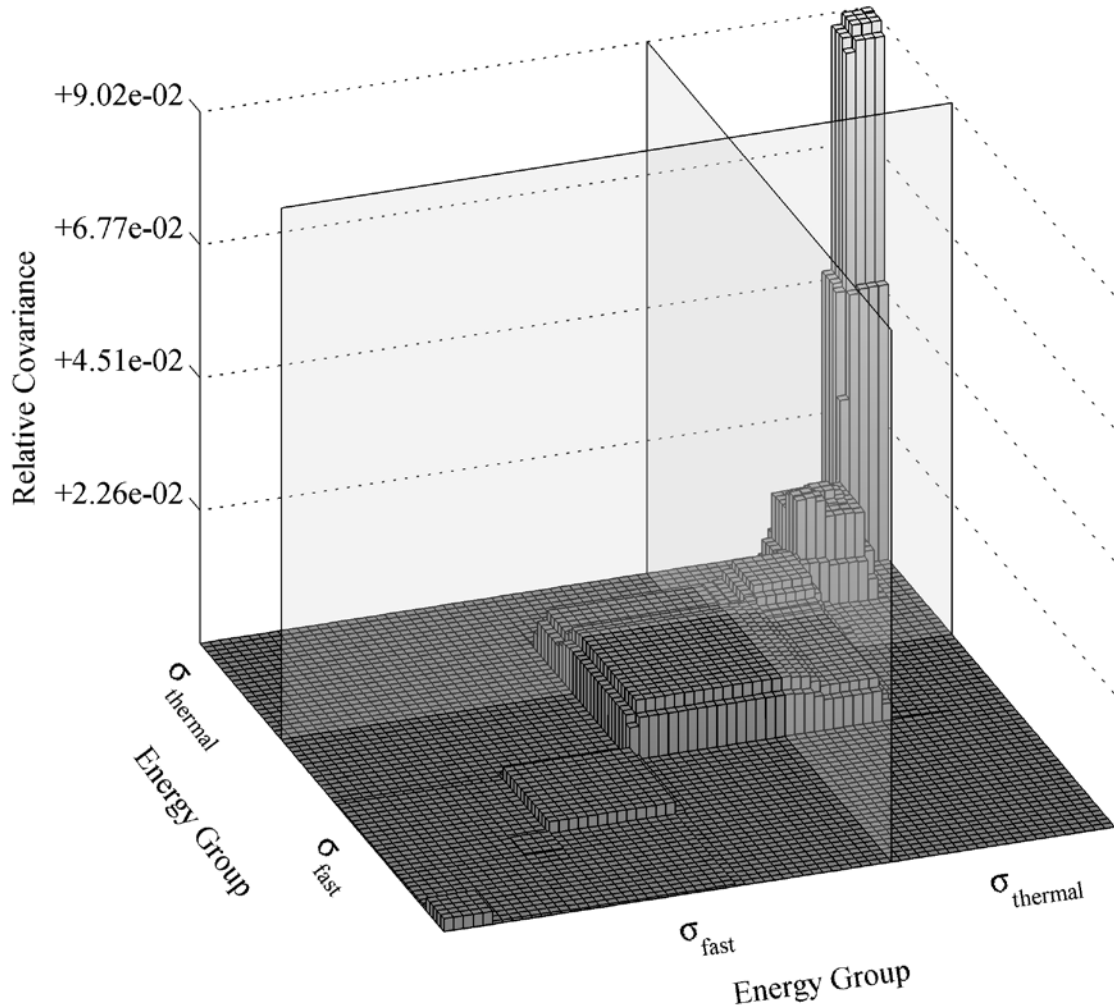


Figure 3 Pu²³⁹ (n, γ) cross-section covariance in 69 energy groups

3. Simulation and Results

This section describes the conditions of a generic 37-element CANDU[®] test case and specifications of the DRAGON lattice model. Uncertainty results are presented for a BoC lattice, as well as a lattice being irradiated at a constant, high power. Covariance matrices of two-group, homogenized cross-sections for the BoC and EoC fuel are presented in this section, as are uncertainties associated with k_{∞} and atomic number densities of bundle materials as a function of burnup.

3.1 CANDU[®] Simulation and Modelling Parameters

The specifications used for the generic, 37-element CANDU[®] modelling of this work are shown in Table 2 through Table 4.

Parameter	Value
Lattice pitch [cm]	28.575
Fuel pellet diameter [mm]	12.24
Fuel pellet material	UO ₂
Fuel density [g/cm ³]	10.4
Fuel enrichment [w/o]	0.7
Cladding outside diameter [mm]	13.08
Cladding thickness [mm]	0.42
Cladding density	6.44
Cladding material	Zr alloy
Pressure tube material	Zr + 2% Nb alloy
Calandria tube material	Zr alloy
Gap material	CO ₂
Moderator material	D ₂ O

Table 2 Generic CANDU[®] lattice specifications

Material	Nuclide	Percent weight
Zr alloy	Zr ^{Nat}	99.67
	Fe ^{Nat}	0.16
	Cr ^{Nat}	0.11
	Ni ^{Nat}	0.06
Zr + 2% Nb alloy	Zr ^{Nat}	97.50
	Nb ^{Nat}	2.50
Uranium fuel	U ²³⁴	0.00
	U ²³⁵	0.70
	U ²³⁸	99.30
Moderator	D ₂ O	99.8
	H ₂ O	0.2

Table 3 Generic CANDU[®] material compositions

Reactor conditions	Value
Fuel temperature [K]	941.29
Cladding temperature [K]	560.66
Moderator temperature [K]	345.66
Moderator density [g/cm ³]	1.083

Table 4 Generic CANDU[®] operating temperatures

Lattice cell	BoC	EoC
Generic CANDU [®]	1.12061	0.987236

Table 5 Best-estimate predictions of generic CANDU[®] k_{∞}

3.1.1 DRAGON Discretization of the Generic CANDU[®] model

The DRAGON transport solution of the generic CANDU[®] model involved a 144-region spatial discretization. The coolant and moderator regions each feature 60 radial divisions, with four radial divisions per fuel pin. Resonance self-shielding is performed on a model of less spatial resolution, consisting of only 28 spatial regions. The transport and self-shielding model discretization schemes are shown in Figure 4.

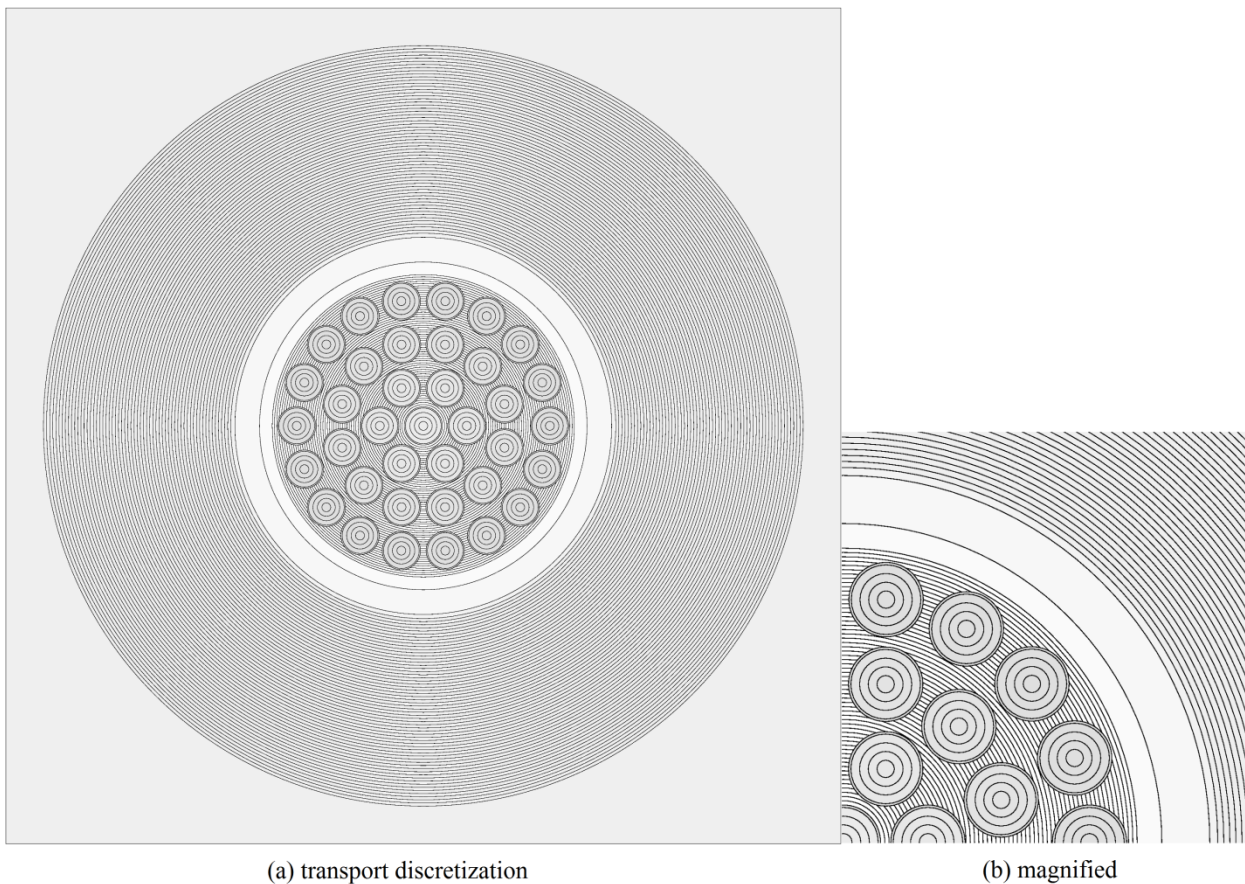


Figure 4 Generic CANDU[®] model discretization for DRAGON transport solution

3.2 Simulation Setup

The generic CANDU[®] model described in section 3.1 was subjected to a DRAGON burnup calculation at a constant, high power for 180 simulated days. The fission power was set constant to 900 kW per bundle. That power is not a reflection of the true power irradiation of in-core bundles in operational CANDU[®] facilities, in which fresh bundles experience a range of power throughout its life, ranging from between one or two hundred Watts to less than 900 Watts. However, the purpose of this burnup investigation is to strictly study the effects of cross-section uncertainties on the production and removal rates of nuclides, and the influence of burnup product cross-section uncertainties on lattice properties.

Cross-section (and other multi-group data) uncertainties were propagated using the statistical sampling method. All the uncertain data was sampled simultaneously from their respective covariance matrices according to an assumed uniform probability distribution. In total, 96 random data sets were generated in this manner, and saved to 96 multi-group data libraries of the WIMS-D4 format. An independent, best-estimate DRAGON burnup calculation was performed on the generic CANDU[®] model for each of the randomly generated WIMS-D4 libraries, producing a set of 96 lattice physics solutions.

Note that nuclear data uncertainties were statistically sampled not only for the nuclides present in the fresh bundle (listed in Table 3) but also for all nuclides that ultimately appear during the burnup sequence, assuming covariance for those nuclides existed. A list of produced nuclides, as calculated using DRAGON and the WLUP IAEA data library is shown in Table 6.

Kr ³⁶	In ¹¹⁵	Nd ¹⁴³	Eu ¹⁵³	Ho ¹⁶⁵	Pu ²⁴⁰
Mo ⁹⁵	Sb ¹²⁵	Nd ¹⁴⁵	Eu ¹⁵⁴	Er ¹⁶⁶	Pu ²⁴¹
Tc ⁹⁹	Te ¹²⁷	Pm ¹⁴⁷	Eu ¹⁵⁵	Er ¹⁶⁷	Pu ²⁴²
Ru ¹⁰¹	I ¹²⁷	Pm ¹⁴⁸	Gd ¹⁵⁴	Pa ²³¹	Am ²⁴¹
Ru ¹⁰³	I ¹³⁵	Pm ¹⁴⁹	Gd ¹⁵⁵	U ²³²	Am ²⁴²
Ru ¹⁰⁶	Xe ¹³¹	Sm ¹⁴⁷	Gd ¹⁵⁶	U ²³³	Am ²⁴³
Rh ¹⁰³	Xe ¹³⁴	Sm ¹⁴⁸	Gd ¹⁵⁷	U ²³⁴	Cm ²⁴²
Rh ¹⁰⁵	Xe ¹³⁵	Sm ¹⁴⁹	Gd ¹⁵⁸	U ²³⁶	Cm ²⁴³
Pd ¹⁰⁵	Xe ¹³⁶	Sm ¹⁵⁰	Dy ¹⁶⁰	U ²³⁷	Cm ²⁴⁴
Pd ¹⁰⁷	Cs ¹³³	Sm ¹⁵¹	Dy ¹⁶¹	Np ²³⁷	
Pd ¹⁰⁸	Cs ¹³⁴	Sm ¹⁵²	Dy ¹⁶²	Np ²³⁹	
Ag ¹⁰⁹	Cs ¹³⁵	Eu ¹⁵¹	Dy ¹⁶³	Pu ²³⁸	
Cd ¹¹³	Cs ¹³⁷	Eu ¹⁵²	Dy ¹⁶⁴	Pu ²³⁹	

Table 6 Nuclides that appear in generic CANDU[®] burnup

3.3 Results

During the burnup calculation of the statistical samples of data sets, multiple lattice responses of interest were recorded, including k_{∞} , two-group homogenized cross-sections, and the total bundle inventory of all 82 lattice nuclides. As there are 96 sets of values for each of those responses,

probability distributions emerged that facilitated the calculation of uncertainties (relative standard deviation), and confidence limits associated with their best-estimate predictions.

3.3.1 Multiplication Constant Uncertainty

The best-estimate lattice multiplication constant, k_{∞} , is shown in along with its 95th percentile confidence limits, as calculated using Wilks' formula. The relative standard deviation of k_{∞} is shown in Figure 6.

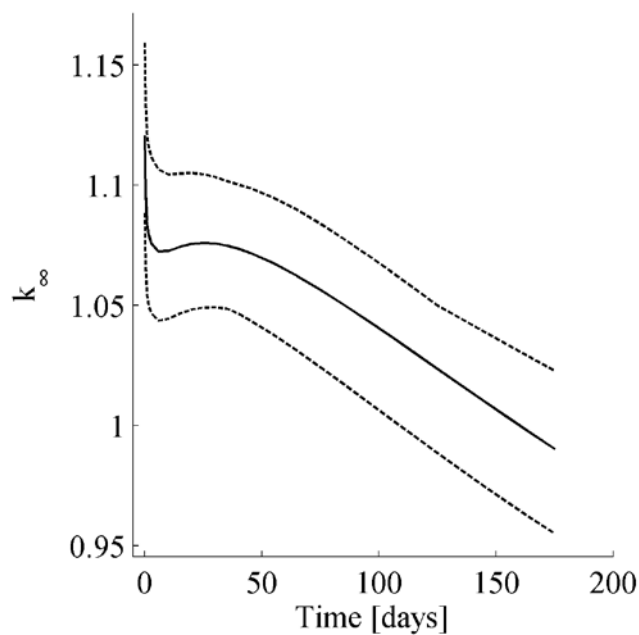


Figure 5 CANDU[®] k_{∞} vs. burnup, with 95th percentile confidence limits

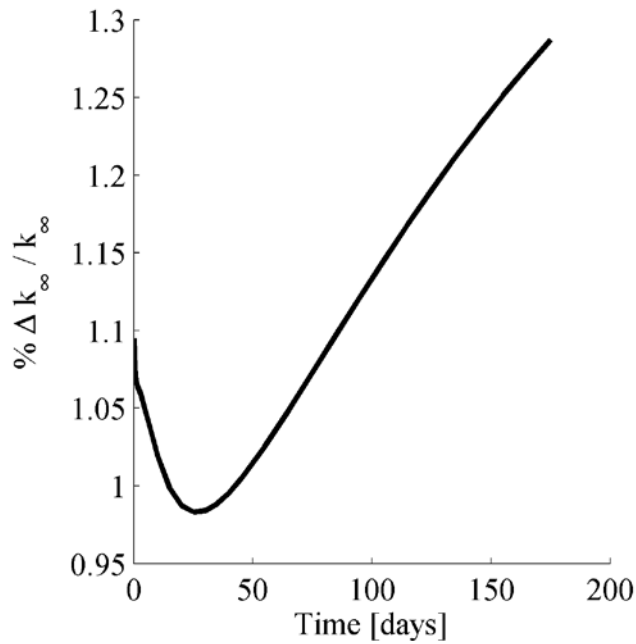


Figure 6 CANDU[®] k_{∞} uncertainty vs. burnup

3.3.2 Homogenized, Two-Group Property Covariance

At both the onset of irradiation at the BoC as well as at the end of the 180 day burnup, lattice properties were homogenized in space and collapsed to a two-group energy structure. The resulting two-group homogenized cross-sections are a primary calculation product of lattice physics, used in subsequent full-core analysis employing diffusion theory. The two-group cross-sections of interest in this work are the total cross-section (Σ_t), scattering cross-section (Σ_s), absorption cross-section (Σ_a), and fission-yield cross-section (Σ_{vf}). The covariance matrix associated with these homogenized cross-sections was calculated at BoC and EoC, and are shown in Figure 7 and Figure 8, respectively.

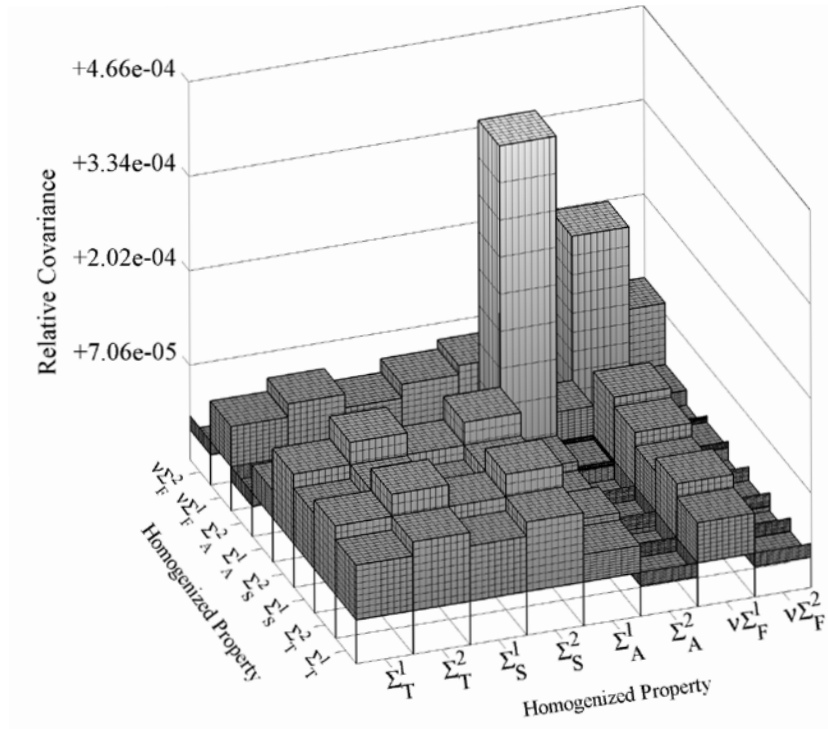


Figure 7BoC few-group property covariance matrix

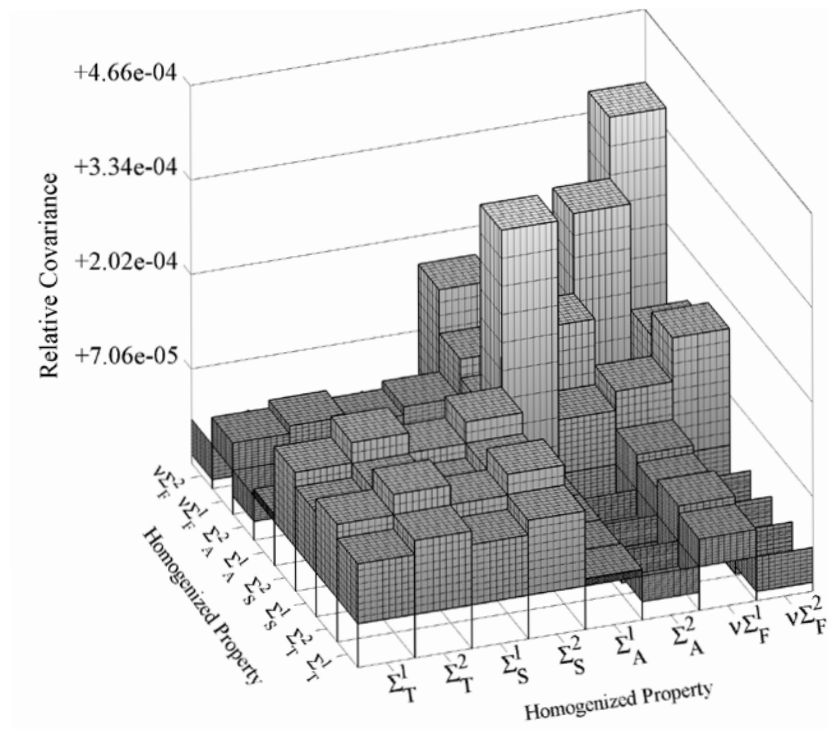


Figure 8EoC few-group property covariance matrix

3.3.3 Nuclide Mass Uncertainty

As illustrated in Figure 1, the confidence associated with quantifying atom densities of lattice nuclides evolves during burnup, a consequence of uncertainties that compound with each timestep. Significant uncertainty was found to exist in the prediction of the accumulated mass of some nuclides. Figure 9 shows 96 predictions of selected nuclide mass that correspond to each of the statistical samples taken of the nuclear data library. More detailed plots, showing both the reference best-estimate prediction of nuclide concentration (lattice volume averaged) of various nuclides as well as their 95th percentile confidence limits are shown in Figure 10 through Figure 23.

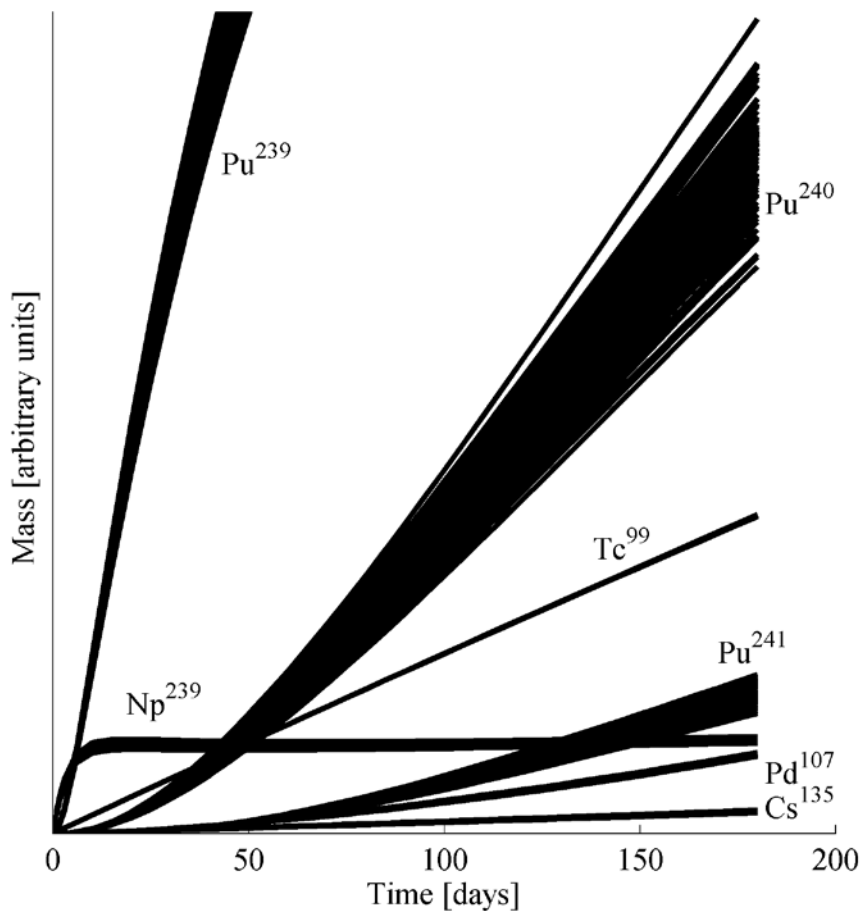


Figure 9 CANDU statistical samples of selected nuclide mass

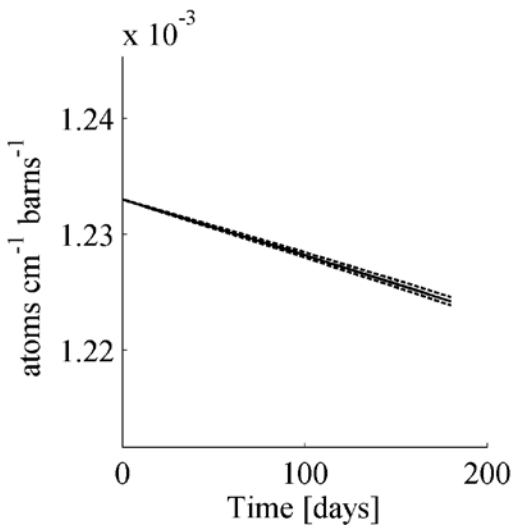


Figure 10 U²³⁸ concentration vs. burnup

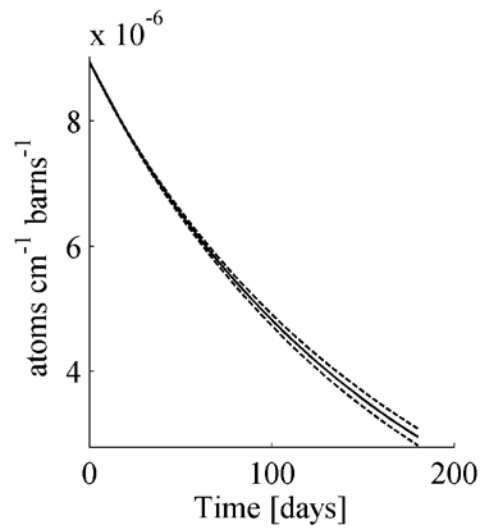


Figure 11 U²³⁵ concentration vs. burnup

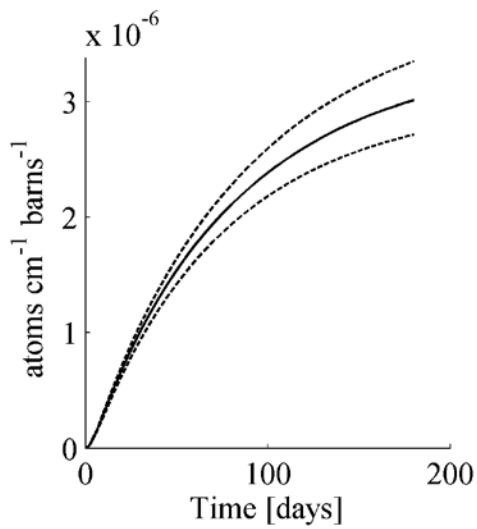


Figure 12 Pu²³⁹ concentration vs. burnup

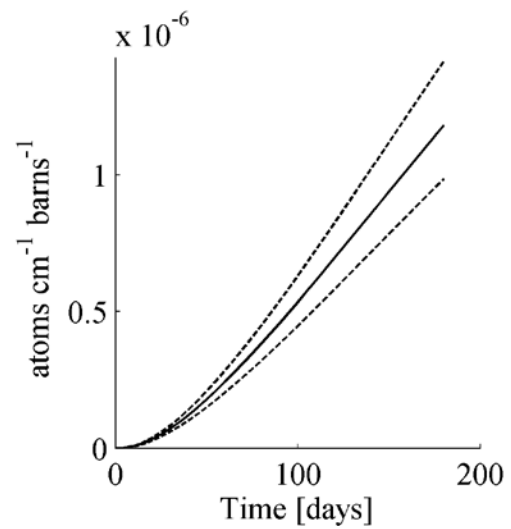


Figure 13 Pu²⁴⁰ concentration vs. burnup

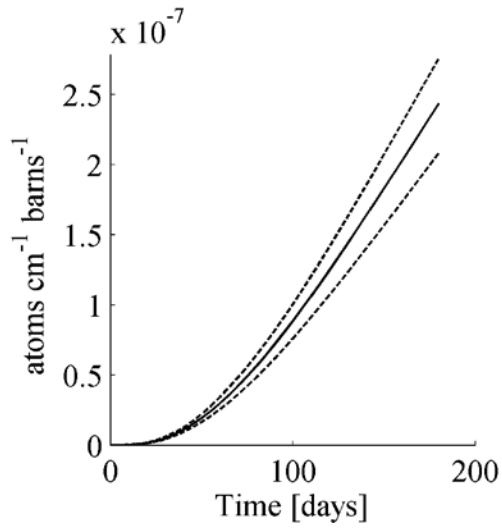


Figure 14 Pu^{241} concentration vs. burnup

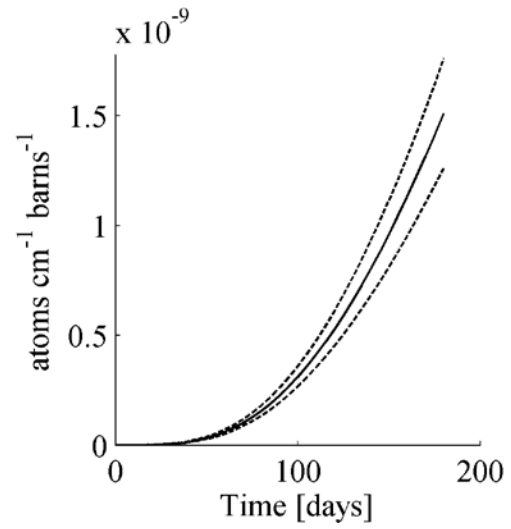


Figure 15 Am^{241} concentration vs. burnup

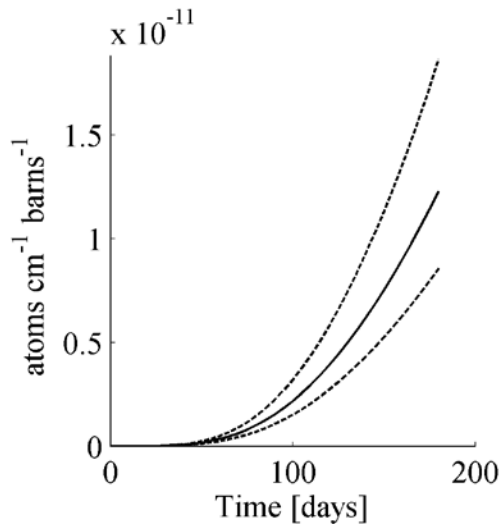


Figure 16 Am^{242} concentration vs. burnup

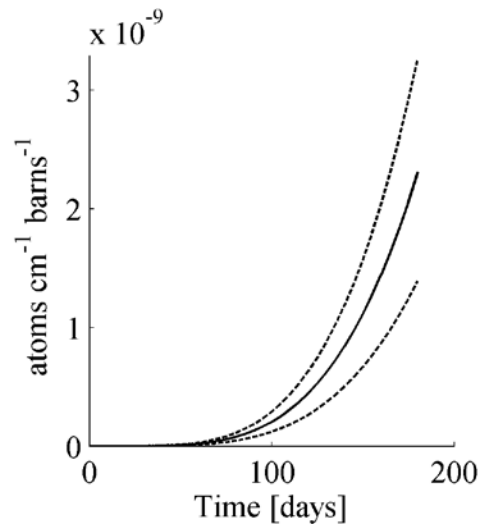


Figure 17 Am^{243} concentration vs. burnup

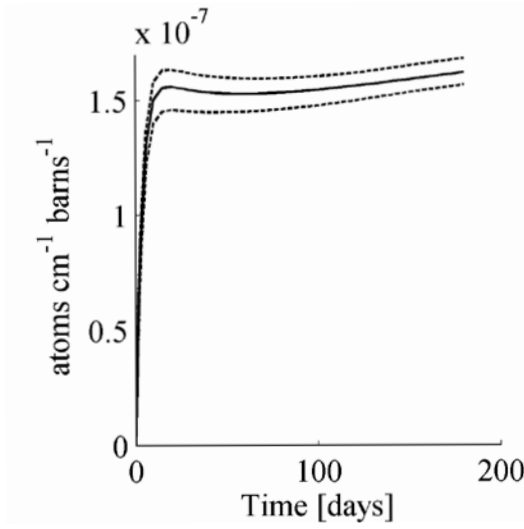


Figure 18 Np^{239} concentration vs. burnup

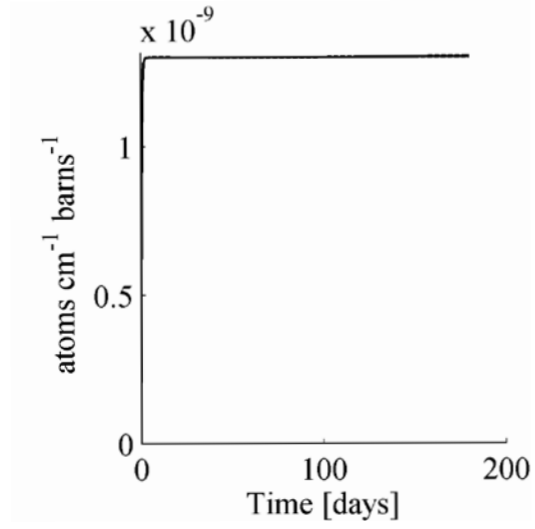


Figure 19 I^{135} concentration vs. burnup

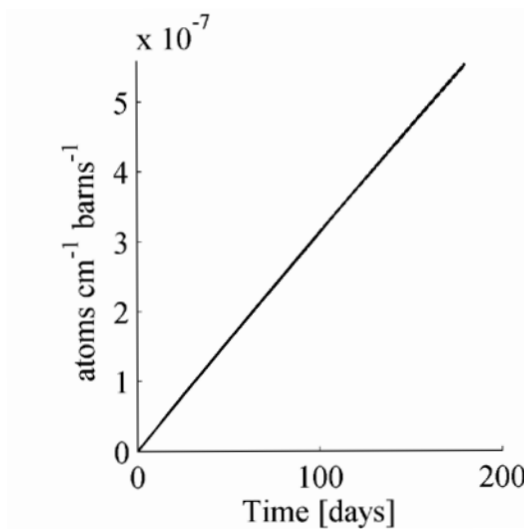


Figure 20 Tc^{99} concentration vs. burnup

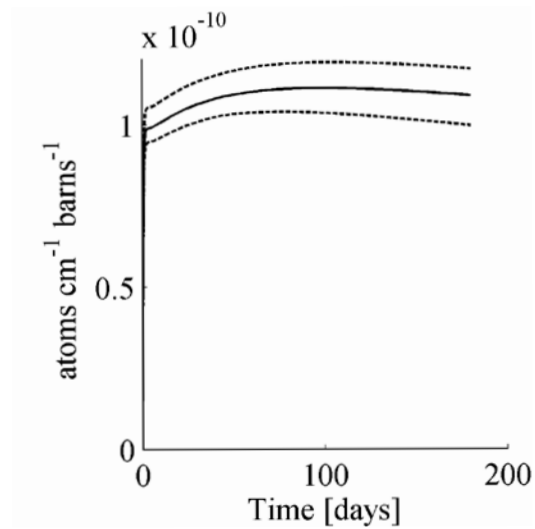


Figure 21 Xe^{135} concentration vs. burnup

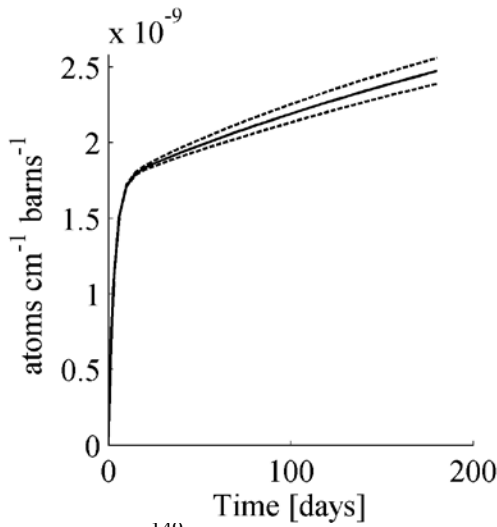


Figure 22 Sm^{149} concentration vs. burnup

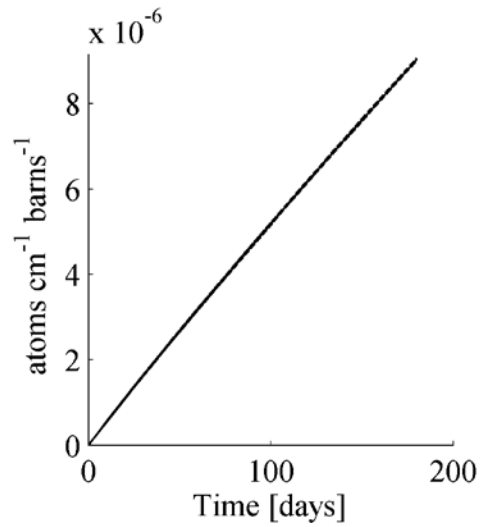


Figure 23 Lumped Fission Product concentration vs. burnup

4. Discussion

Despite that the fission yield fractions and decay rates of nuclides on the IAEA data library were not involved in the statistical sampling (because uncertainty associated with those parameters was unavailable), substantial uncertainty was observed during burnup due solely to the multi-group covariance associated with microscopic cross-sections.

At the onset of burnup, k_{∞} declines rapidly as fission product poisons emerge. When at constant power, the quickly-decaying poison nuclides will gradually achieve steady-state concentrations, including, notably, Xe^{135} , which was found to do so in this study after several days. Simultaneously, Pu^{239} , resulting from neutron capture by U^{238} , accumulates in the fuel and its large fission-to-capture ratio offers an improvement to reactivity that briefly outweighs the poison effect of fission products resulting in the well-known “plutonium peak”. While many fission products are explicitly included in the IAEA data library, many are aggregated into a single virtual nuclide referred to as a Lumped Fission Product (LFP). The nuclides that constitute the LFP are shown in Table 7, and the rationale behind the selection of LFP nuclides can be found in WLUP literature[6]. Because the LFP is not an isotope, it has no corresponding covariance in the 44GROUPV6REC uncertainty library. A covariance matrix for the LFP could be constructed if the weighting function applied its constituent nuclides was well known, but in the absence of such information, no covariance could reasonably be assembled.

Ge^{72}	Kr^{84}	Nb^{94}	I^{113}	Te^{130}	Nd^{144}
Ge^{73}	Kr^{86}	Mo^{96}	Sn^{115}	I^{129}	Nd^{146}
Ge^{74}	Rb^{85}	Mo^{97}	Sn^{117}	Xe^{128}	Nd^{147}
Ge^{76}	Rb^{87}	Ru^{99}	Sn^{118}	Xe^{130}	Nd^{150}
As^{75}	Sb^{86}	Ru^{100}	Sn^{119}	Xe^{132}	Sm^{154}
Se^{76}	Sb^{87}	Ru^{102}	Sn^{126}	Ba^{134}	Gd^{152}

Se ⁷⁷	Sr ⁸⁸	Ru ¹⁰⁴	Sb ¹²¹	Ba ¹³⁵	Gd ¹⁶⁰
Se ⁷⁸	Y ⁸⁹	Pd ¹⁰⁴	Sb ¹²³	Ba ¹³⁶	Tb ¹⁵⁹
Se ⁸⁰	Zr ⁹⁰	Pd ¹⁰⁶	Te ¹²²	Ba ¹³⁷	Tb ¹⁶⁰
Se ⁸²	Zr ⁹¹	Pd ¹¹⁰	Te ¹²³	Ba ¹³⁸	
Br ⁷⁶	Zr ⁹²	Cd ¹¹¹	Te ¹²⁴	Ce ¹⁴⁰	
Br ⁸¹	Zr ⁹³	Cd ¹¹²	Te ¹²⁵	Ce ¹⁴²	
Kr ⁸⁰	Zr ⁹⁴	Cd ¹¹⁴	Te ¹²⁶	Pr ¹⁴¹	
Kr ⁸²	Zr ⁹⁶	Cd ¹¹⁶	Te ¹²⁸	Nd ¹⁴²	

Table 7 IAEA LFP contents

The variation of uncertainty associated with k_{∞} can be explained through the changes in concentration of lattice nuclides described above. Notice how the uncertainty of k_{∞} falls sharply after the onset of burnup, and reaches a global minimum of less than 1% $\Delta k_{\infty}/k_{\infty}$ at 30 days of irradiation, which corresponds to approximately 1200 MW-days/tonne of burnup. This drop in uncertainty is not correlated with the concentration of any one particular isotope, but instead emerges from a complex set of competing phenomena involving several isotopes. The behaviour of $\Delta k_{\infty}/k_{\infty}$ has two dominant features: the decline during the first 30 days followed by a steady rise.

The initial drop in uncertainty is due to the rapid accumulation of fission products at the onset of burnup. As their concentrations grow, they become responsible for an increasing frequency of parasitic absorptions of neutrons, which dulls the sensitivity of k_{∞} to $U^{238}(n, \gamma)$. Fission product absorption covariance, however, tends to be substantially less than that of $U^{238}(n, \gamma)$. Therefore, in terms of the total absorption rate, high-uncertainty captures by U^{238} are substituted with low-uncertainty captures of fission product nuclides such as Xe^{135} , Sm^{149} as well as the LFP which has no known covariance. Further into burnup, as Plutonium concentrations grow, the inverse change of uncertainty occurs. Plutonium nuclides have much larger fission cross-section uncertainty than does U^{235} . Therefore, low-uncertainty fission rates of U^{235} are substituted by high-uncertainty fission rates of Pu^{239} . After approximately 30 days of burnup, the increased Plutonium fission rate uncertainty leads to a continually increasing uncertainty of k_{∞} .

Regarding the covariance of the two-group, homogenized lattice properties, a large reduction of fast-group absorption uncertainty can be seen in the EoC case in Figure 8 compared to the BoC case in Figure 7. Also, after burnup, a large increase is seen in fission-yield cross-section in both energy groups. No significant change in covariance is observed in the scattering cross-section, as lattice-homogenized scattering is dominated almost exclusively by moderator nuclides, whose atom densities are invariant with fuel irradiation.

5. Conclusions

The new tool developed by the authors to conduct lattice uncertainty propagation using a statistical sampling method proved well-suited to quantifying of lattice covariance during burnup.

It was found that even when uncertainties associated with fission yield fractions and radionuclide decay rates were neglected, microscopic cross-section uncertainties resulted in a substantial loss of

confidence associated with best-estimate predictions of k_{∞} and nuclear reactor product masses of the lattice cell. However, additional study must be performed in which the covariance of the WLUP lumped fission product virtual nuclide is adequately assessed and included in the uncertainty analysis.

6. References

- [1] K. Ivanov, et al., “Benchmark for Uncertainty Analysis in Modeling (UAM) for Design, Operation and Safety Analysis of LWRs”, OECD Nuclear Energy Agency, Vol. I, Version 2.0, February 2011.
- [2] M. R. Ball, “Uncertainty Analysis in Lattice Reactor Physics Calculations”, Doctoral Thesis, 2011.
- [3] Brookhaven National Laboratory, “ENDF-6 Formats Manual: Data Formats and Procedures for the Evaluated Nuclear Data File ENDF/B-VI and ENDF/B-VII”, Document ENDF-102, June 2009.
- [4] Oak Ridge National Laboratory, “SCALE 5.1 Cross-Section Covariance Libraries”, ORNL/TM-2005/39, Version 5.1, Rev. 1, Vol I, Book 3, Sec. M19, February 2008.
- [5] G. Marleau, A. Hebert, R. Roy, “A User Guide for DRAGON 3.06”, Technical Report, IGE-236, Revision 1, EcolePolytechnique de Montreal, October 2001.
- [6] International Atomic Energy Agency, “WIMS-D Library Update: Final Report of a Coordinated Research Project”, Vienna, 2007.
- [7] I. Kodeli, “Manual for ANGELO2 and LAMBDA Codes”, NEA-1798 Package, 2008.